



Article

Efficiency Enhancement in Double-Pass Perforated Glazed Solar Air Heaters with Porous Beds: Taguchi-Artificial Neural Network Optimization and Cost–Benefit Analysis

Roozbeh Vaziri ^{1,*}, Akeem Adeyemi Oladipo ^{2,*}, Mohsen Sharifpur ^{3,4,5,*} , Rani Taher ⁶ ,
Mohammad Hossein Ahmadi ^{7,*} and Alibek Issakhov ⁸

¹ Faculty of Engineering, Cyprus Science University, TRNC via Mersin 10, Kyrenia 99300, Turkey

² Polymeric Materials Research Laboratory, Chemistry Department, Faculty of Arts and Science, Eastern Mediterranean University, TRNC via Mersin 10, Famagusta 99450, Turkey

³ Department of Mechanical and Aeronautical Engineering, University of Pretoria, Pretoria 0002, South Africa

⁴ Department of Medical Research, China Medical University Hospital, China Medical University, Taichung 404, Taiwan

⁵ Department of Mechanical Engineering, Faculty of Engineering, University of Science and Culture, Tehran 1461968151, Iran

⁶ College of Engineering and Technology, American University of the Middle East, 220 Dasman, Egaila 15453, Kuwait; rani.taher@aum.edu.kw

⁷ Faculty of Mechanical Engineering, Shahrood University of Technology, Shahrood 3619995161, Iran

⁸ Department of Mathematical and Computer Modelling, Faculty of Mechanics and Mathematics, Al-Farabi Kazakh National University, Almaty 050040, Kazakhstan; Alibek.Issakhov@kaznu.kz

* Correspondence: roozbehvaziri@csu.edu.tr (R.V.); akeem.oladipo@emu.edu.tr (A.A.O.); mohsen.sharifpur@up.ac.za (M.S.); mhosein.ahmadi@shahroodut.ac.ir (M.H.A.)



Citation: Vaziri, R.; Oladipo, A.A.; Sharifpur, M.; Taher, R.;

Ahmadi, M.H.; Issakhov, A. Efficiency Enhancement in Double-Pass Perforated Glazed Solar Air Heaters with Porous Beds: Taguchi-Artificial Neural Network Optimization and Cost–Benefit Analysis. *Sustainability* **2021**, *13*, 11654. <https://doi.org/10.3390/su132111654>

Academic Editor:
Jesús Las-Heras-Casas

Received: 10 August 2021
Accepted: 18 October 2021
Published: 21 October 2021

Publisher's Note: MDPI stays neutral with regard to jurisdictional claims in published maps and institutional affiliations.



Copyright: © 2021 by the authors. Licensee MDPI, Basel, Switzerland. This article is an open access article distributed under the terms and conditions of the Creative Commons Attribution (CC BY) license (<https://creativecommons.org/licenses/by/4.0/>).

Abstract: Analyzing the combination of involving parameters impacting the efficiency of solar air heaters is an attractive research areas. In this study, cost-effective double-pass perforated glazed solar air heaters (SAHs) packed with wire mesh layers (DPGSAHM), and iron wools (DPGSAHI) were fabricated, tested and experimentally enhanced under different operating conditions. Forty-eight iron pieces of wool and fifteen steel wire mesh layers were located between the external plexiglass and internal glass, which is utilized as an absorber plate. The experimental outcomes show that the thermal efficiency enhances as the air mass flow rate increases for the range of 0.014–0.033 kg/s. The highest thermal efficiency gained by utilizing the hybrid optimized DPGSAHM and DPGSAHI was 94 and 97%, respectively. The exergy efficiency and temperature difference (ΔT) indicated an inverse relationship with mass flow rate. When the DPGSAHM and DPGSAHI were optimized by the hybrid procedure and employing the Taguchi-artificial neural network, enhancements in the thermal efficiency by 1.25% and in exergy efficiency by 2.4% were delivered. The results show the average cost per kW (USD 0.028) of useful heat gained by the DPGSAHM and DPGSAHI to be relatively higher than some double-pass SAHs reported in the literature.

Keywords: perforated solar air heater; glazed solar collector; thermal efficiency; wire mesh; double-pass collector

1. Introduction

Recently, concerted interests have been directed toward renewable energy conversion systems due to their potential in providing a sustainable future. Solar collectors (water/air) are widely applied in various thermal equipment for the optimal and efficient utilization of solar energy. The conventional solar air heaters (SAHs) consist of a solar radiation absorber plate and a parallel plate below through which the inlet air is heated and obtained hot air utilized for various applications, such as greenhouse heating, curing of concrete building components and seasoning of timber [1–3]. The conventional SAHs are cheap, simple in design and require little maintenance [4].

Despite the numerous areas of application, the conventional SAHs have less heat storage capability and thus exhibited relatively low thermal efficiency attributed to various controllable (collector materials, absorber plate and depth of bed) and uncontrollable factors (solar intensity, wind speed, humidity and ambient temperature) [5–7]. To this end, increasing efforts have been focused on the enhancement of thermal performance and the total general SAH efficiency. Application of extended/corrugated surfaces, the double-pass solar air heater (DPSAH) with packed bed, perforated glazed absorber and using porous material inside the collector are a few examples of these modifications to enhance the heat transfer coefficient inside the collector and to improve the SAH performance [5,6,8,9]. Alta et al. [2] investigated various models of SAHs. They showed that the thermal efficiency of SAH with obstacles attached to the absorber plate is higher than those without obstacles. The use of porous media (iron wools, wire mesh, gravels and limestone) tends to significantly increase the turbulence of air streams and the ratio of surface area to unit volume [10,11]. Paisarn [12] reported that the thermal efficiency of a double-passed SAH with porous media is higher (42–70%) than that without a porous medium (38–59%).

Therefore, the controllable factors (collector materials, absorber plate and depth of bed) play a significant role in the SAH performance. Practically, an accurate mechanism to predict the values of the uncontrollable factors is necessary for a comprehensive and precise estimation of the performance of the SAH with minimal experimental flaws and design. The thermodynamic and experimental analysis of SAH is complicated due to the numerous measurements and heat transfer processes. To solve these issues, many studies have focused on predicting both controllable and uncontrollable factors that contribute toward the thermal performance of SAHs, particularly using various analytical computer codes and optimization algorithms [13,14].

According to [15], the authors applied a technique of machine learning regression to estimate thermal efficiency and heat transfer of a helical corrugation with perforated circular disc SAH tubes. Alam and Souayeh [16] conducted a numerical investigation on thermo-hydraulic characteristics, which lead to increasing the heat transfer in SAH.

Panda et al. [17] employed a finite difference method (FDM) and binary-coded genetic algorithm (GA) to optimize the controllable characteristics parameters (thermal conductivity of the absorber plate, incident solar heat flux and overall heat loss coefficient) in a flat-plate solar system to achieve a given temperature field. Using this combined optimization approach, the authors proposed varying locations and suitable materials for the absorber plate satisfying the prescribed temperature field in the collector. Similarly, Das et al. [18] applied an artificial bee colony (ABC) algorithm to optimize five influencing parameters affecting the heat loss factor of a double glazed solar collector in the domestic water heating system. After using the ABC algorithm, the authors reduced the size of the collector by 6–32% and introduced absorber plate emissivity as an important parameter to control the heat loss factor of the double-glazed collector.

Even though the use of some of these analytical computer codes or optimization algorithms (ABC, FDM etc.) has achieved reasonable results, they are slow. The software is relatively expensive, requires a high amount of computing power and often involves complex differential equations. To avoid complex solutions and time-consuming routines, artificial intelligence and Taguchi's analysis-based models have proven to be a cheaper and accurate alternative to tackling these problems.

Unlike the ABC, the Taguchi technique reduces variation in a process through the robust design of experiments. In addition, its data exploration and exploitation behavior are quick, making it helpful in manufacturing industries.

The Taguchi methodology involves using orthogonal arrays (OA) to classify the parameters influencing a process and the levels at which these parameters should be varied and are more efficient than ABC's multistep system exploration [19,20]. The Taguchi methodology tests pairs of combinations of data to investigate which factors most influence product efficiency with a minimum amount of experimentation, thus saving resources and time [20]. Kuo et al. [21] applied the Taguchi methodology and grey relational analysis to optimize

the flat-plate collector process. In this study, the authors reported 0.7911 as the efficiency coefficient and $3.470 \text{ W}/^\circ\text{C m}^2$ as the heat dispersion factor under optimal conditions. By using the Taguchi method, the experimental time and costs were greatly reduced.

In the last decade, the utilization of artificial intelligence methods in scientific and engineering experiments has been gradually increasing. The artificial neural network (ANN) model is relatively fast and, by using trained parameters (inputs, weights and biases), can solve complex problems and estimate target data of various systems, including the thermal systems in engineering applications with high accuracy [19,22]. Omojaro et al. [23] applied ANN to train and test measurable controlled and conditional factors of a single pass SAH. For the tested network, the authors reported an average thermal efficiency of 43.7% and mean square error of 0.0036, and the variation in the efficiency of the neural network was 2.032% when compared with physical experimental data. The obtained results indicate that ANN can be a useful tool for estimating both conditional and unconditional factors of SAHs with reasonable accuracy to design effective, economical and high-performance SAH.

Ghritlahre and Prasad [24] presented the different models of ANN technique to anticipate the thermal performance of unidirectional flow porous bed solar air heater.

Furthermore, Ghritlahre et al. [25] utilized the ANN technique to predict the thermal performance of two various types of SAHs. Additionally, their study illustrated that the air mass flow rate has a drastic effect on the efficiency of SAH among the sensitive input parameters.

The scholars obtained that the thermo-hydraulic performance of a solar air heater with circular perforated absorber plate could be predicted by utilization of ANN [26].

The objective of the present work was to use a Taguchi methodology for the design and selection of the right configuration of double-pass perforated glazed solar air heaters with porous materials (iron wool and wire mesh) as absorbers. The Taguchi method was used to maximize the efficiency of the as-fabricated SAHs by determining the optimum combination of various system parameters. Then, data from uncontrollable input variables were fed into the ANN to predict the efficiency of the optimized SAHs.

According to the literature review, several researchers have worked on SAHs with effective absorber designs to increase their thermal performance. Despite the vast research on solar air heaters, the bulk of these studies only consider a single parameter (such as the roughness or porosity of the absorber plate) while keeping the other factors constant. As a result, the combined influence of various parameters was not taken into account. The most novel aspect of this report is the comprehensive assessment of combined parameters impacting the efficiency of double-pass perforated glazing solar air heaters with different porous materials using two widely used modeling tools. This method is broadly acknowledged as a useful tool for determining the best performance of solar air heaters while remaining cost-effective and environmentally friendly.

2. Experimental Setup

In this study, the efficiency of two different configurations of double-pass perforated glazed SAH packed with iron wools (DPGSAHI) and mesh layers (DPGSAHM) (Figure 1) were experimentally investigated at Famagusta, North Cyprus (35.13° North latitude, 33.95° East longitude and 1 m elevation above the sea level). The experiments were accomplished on clear sunny days using each SAH configuration at varying air mass flow rates (0.014–0.033 kg/s). The double-pass perforated glazed SAHs (DPGSAH) is $90 \text{ cm} \times 90 \text{ cm}$ in dimension and consists of perforated plexiglass (PG) as a glazed cover, a normal glass inside the collector, radial fan and mesh layers, or iron wools were utilized as packed beds. The packing materials were painted black to enhance absorptivity, and the SAHs were insulated by 3 cm dark-coloured thick polystyrene to decrease the heat losses significantly.

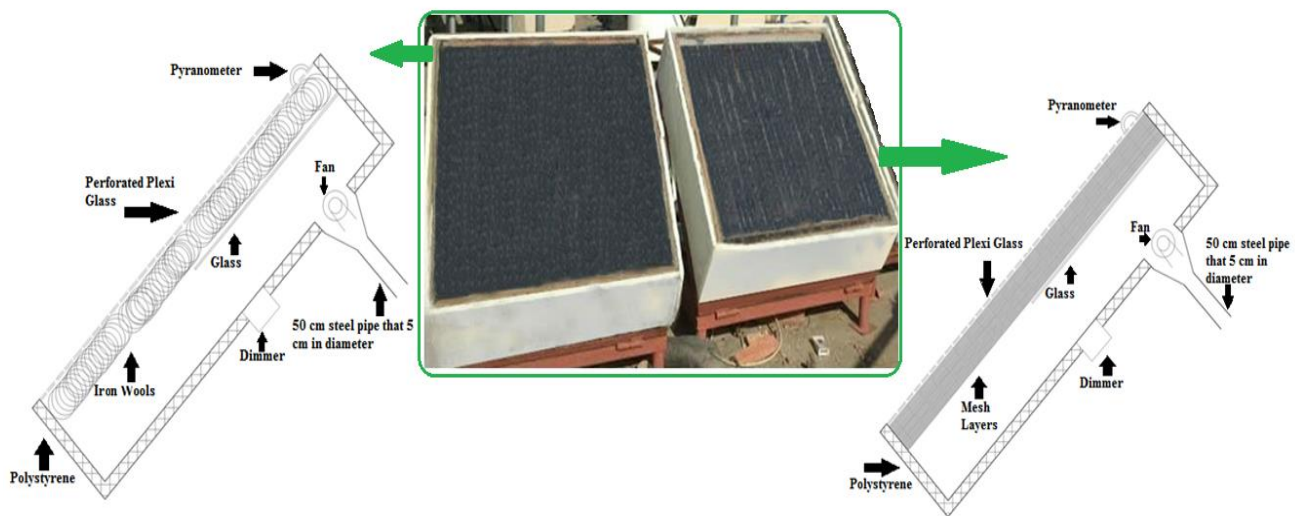


Figure 1. Schematic and actual picture of optimized DPGSAHI and DPGSAHM.

The dimensions of PG are $(88 \times 88) \text{ cm}^2$, and the diameter of holes in PG is 3 mm with pitch (distance between holes) of 3 cm. A standard glass of 3 mm thick with dimensions of $(85 \times 60) \text{ cm}^2$ is inserted inside the DPGSAH at 10 cm from the PG as schematically shown in Figure 1. The DPGSAHM consists of 15 blackened steel wire mesh layers with $1.2 \times 1.2 \text{ cm}^2$ in cross-section voids and 0.085 cm in diameter of wire situated parallel between the upper side of normal glass and back of the PG. The distance between each mesh layer is 0.5 cm. The DPGSAHI has 60 blackened iron pieces of wool located between the upper side of the normal glass and the backside of PG.

The packing materials were systematically arranged in layers to provide high porosity, $\varnothing = 95.2\text{--}98.3\%$ and thus decreased the pressure drop through the collector significantly as measured by the inclined manometer. The air flow was circulated by the 250 W PV-powered radial fan situated at the backside of the collector, and a 50-cm pipe was installed on the outlet of the radial fan to reduce turbulent flow. The tests were conducted under actual conditions.

3. Experimental Data Modeling: Taguchi Methodology and Artificial Neural Network

3.1. Taguchi Methodology

Taguchi methodology is extensively utilized in engineering problems via the application of statistical and engineering concepts to achieve desired product efficiency. The Taguchi design method applies a mathematical tool called orthogonal arrays (OAs) and signals to noise (S/N) ratio to study experimental design techniques and factors variations with product efficiency [19,27,28]. Taguchi suggests a three-phase process flow: system design, parameter design and tolerance design [28]. The parameter design is the key thrust of Taguchi's approach; here, the variables are experimentally analyzed to determine how the process reacts to uncontrollable "noise" in the system [27].

In Taguchi's parameter design stage, an experimental design is employed to arrange the control and noise factors in the inner and outer orthogonal arrays, respectively. Thereafter, the S/N ratio for each experimental combination is computed and analyzed to determine the optimal control factor level. Three different computation equations for the S/N ratio have been suggested depending on the characteristics as follows: smaller-is-better, nominal-is-better and larger-is-better [19,27]. The quality characteristics discussed herein are efficiency (thermal and exergy) and outlet air temperature of the SAH. Higher efficiency is desired; hence, the larger-the-better characteristic is chosen and expressed as follows:

$$SNR = -10 \log_{10} \left(\frac{1}{n} \sum_{i=1}^n \frac{1}{y_i^2} \right) \quad (1)$$

which y is the response and n is the number of tests in a level combination. The levels of various control factors used in this experiment are presented in Table 1. The Taguchi analysis is performed with Quantum XL 2016 (SigmaZone, Orlando, FL, USA) software package, and the L_8 orthogonal array has been chosen for the present empirical study. In traditional full factorial experiment design, the seven controllable factors each at two levels would require $6^2 = 36$ runs to study the different factors. However, Taguchi's robust approach decreased it to 8 runs, offering a better advantage in terms of experimental time and cost. The optimized observed responses were determined by comparing the standard method and analysis of variance (ANOVA).

Table 1. Parameter factors of the perforated glazed SAHs and their levels in the Taguchi design.

Control Factor	Unit	Levels	
		1	2
A: Type of absorber material		Iron wool	Wire mesh
B: Gap between internal glass and plexi glass	cm	7	10
C: Thickness of packing material	cm	0.07	0.1
D: Diameter of holes of plexi glass	mm	1	3
E: Distance between absorber material	cm	0.1	0.5
F: Thickness of bottom insulation	cm	2	4

3.2. Artificial Neural Network

Artificial neural network (ANN) is inspired by the way biological nervous systems (brain) process information [29]. The ANN usually consists of an input layer, hidden layer and an output layer. The network is trained by adjusting weight connections between the neurons until maximum epochs are reached [22], and like people, ANNs learn by example.

In the present work, the SAH systems modelled by the ANN had four inputs and three outputs, as presented in Table 2. All network calculations were performed using Neuroph 2.94 software. 89 datasets were fed into the network, which from them, 65 data were used for training, 15 for testing and the remaining 9 were used as the validated data set. To enhance the training process and the network's generalization capabilities, whole input information was normalized to quantities between 0.12 and 0.98 using Equation (2). Here, X_n represents the normalized value, X_0 is the actual value of input variables, and X_{max} and X_{min} are the maximum and minimum values of input variables, respectively.

$$X_n = \left(\frac{X_0 - X_{min}}{X_{max} - X_{min}} \right) \times (0.98 - 0.12) + 0.12 \quad (2)$$

Table 2. ANN training parameters and the area of variation of input and output data.

		The Area of Variation of Outputs		
Inputs	Range		Iron Wool	Wire Mesh
I (Wm^{-2})	457–990	Outlet air temperature ($^{\circ}C$)	29.3–56.9	28.4–54.6
T_{air} ($^{\circ}C$)	17.7–28.2	Thermal efficiency (%)	69–91.3	65–85.5
\dot{m} (kg/s)	0.014–0.033	Exergy efficiency (%)	60–71	72–89
Training parameters		Type	NSE	Epoch
The initial weights and biases		Random		
Learning rate		0.7		
Momentum		0.5		
Learning algorithm		Levenberg–Marquardt	0.95904	39
		Scaled conjugate gradient	1.32912	105
		Pola–Ribiere conjugate gradient	2.17591	28
		Batch gradient descent	1.55255	102
		Quasi–Newton method	0.86476	134

NSE: Normalized squared error.

The quasi-Newton method was chosen as the training algorithm because of the lowest normalized squared error of 0.864759, which is lower than other training algorithms shown in Table 2. The plots in Figure 2 show the training and selection errors in each iteration using both Levenberg–Marquardt (LM) and quasi-Newton method (QNM) training algorithms. The blue line represents the training error, and the orange line represents the selection error. For the LM, the initial value of the training error was 1.61517, and the final value after 39 epochs was 0.959036. The initial value of the selection error is 1.90175, and the final value after 39 epochs was 1.11392. While for the QNM, the initial value of the training error was 1.47391, and the final value after 134 epochs was 0.864759. The initial value of the selection error was 1.98173, and the final value after 134 epochs is 0.914968.

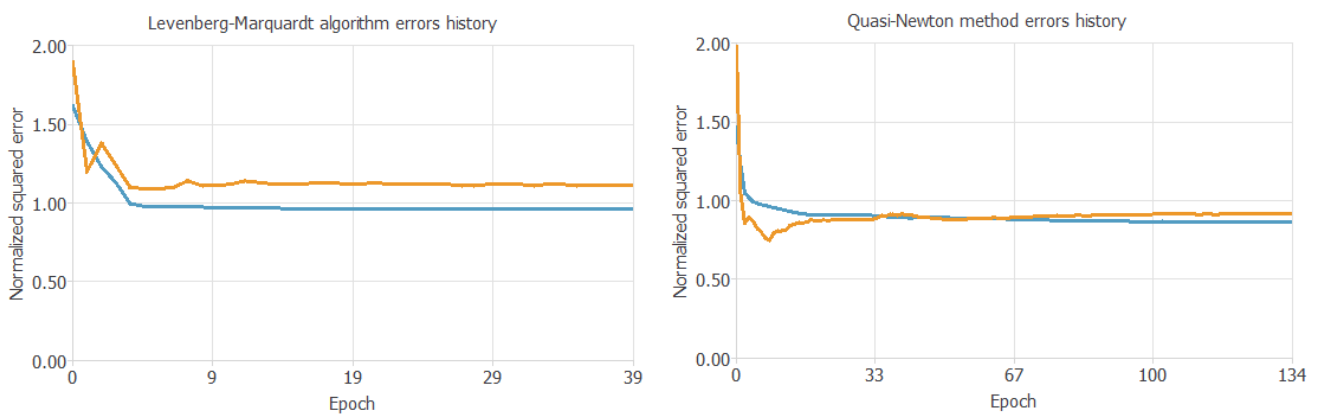


Figure 2. Training and selection errors of experimental data via artificial neural network.

Different network architectures were tested to find the best (Table 2); then, a 3-layered ANN (3:6:3) by logsig activation function at the hidden layer and linear transfer function (purelin) at the output layer was expanded as shown in Figure 3. To characterize prediction efficiency of the optimized ANN architecture, the root mean square error (RMSE) and the coefficient of determinations (R^2) were used to compare the actual experimental and predicted values.

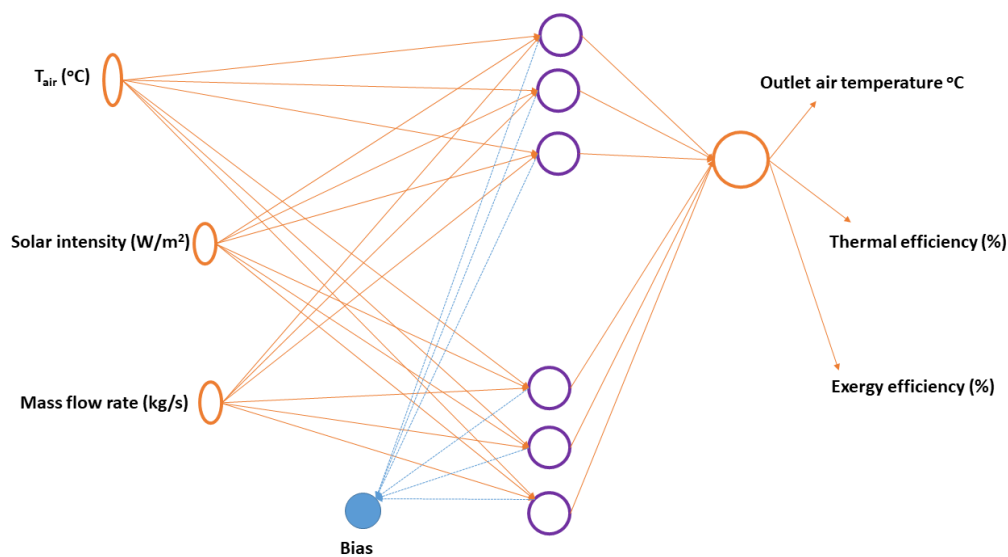


Figure 3. The optimized ANN architecture for predicting the thermal and exergy efficiencies of DPGSAHI and DPGSAHM.

4. Experimental Uncertainty, Energy and Exergy Analysis

Generally, the precision of the experiments is ascertained by uncertainty analysis. In addition, the air temperature, rate of air mass flow and solar intensity were calculated with

devices as described in our recent report [4], and the uncertainties are estimated according to [30]:

$$w_r = \left[\left(\frac{\partial R}{\partial x_1} w_1 \right)^2 + \left(\frac{\partial R}{\partial x_2} w_2 \right)^2 + \dots + \left(\frac{\partial R}{\partial x_n} w_n \right)^2 \right]^{0.5} \quad (3)$$

where R is a certain function and the input variables are x_1, x_2, \dots, x_n , which total uncertainty is w_r , and the uncertainty in the input variables are w_1, w_2, \dots, w_n [9]. The uncertainties in thermal efficiency, outlet air temperature and exergy efficiency are 4.8%, $\pm 2.6\%$ and $\pm 5.4\%$, respectively. The measurements demonstrated the fractional uncertainties for $T_{\text{air}}, V, r, \Delta T$ and I , to be 0.0016, 0.0013, 0.005, 0.025 and 5.7×10^{-6} , respectively.

The efficiency of the SAH, η , was calculated, which is the proportion of obtained energy to incident solar radiance over the collector plate [4]:

$$\eta = \frac{\dot{m}C_p(T_{\text{out}} - T_{\text{in}})}{IA_c} \quad (4)$$

The exergy analysis is based on the two laws of thermodynamics explained in details elsewhere [31], and the following assumptions were considered during the exergy analyses [32]:

- The procedure is conducted in a stable flow operation.
- Air is assumed as an ideal gas with an unchanging specific heat.
- Effects due to the kinetic and potential energy changes are neglected.

The exergetic efficiency is calculated as follows [31,32]:

$$\eta_{\text{ex}} = 1 - \frac{\text{Exergy destroyed}}{\text{Exergy supplied}} \quad (5)$$

Considering the amount of irreversibility in SAH and the negligible pressure drop, the final form of the exergy efficiency can be written as:

$$\eta_{\text{ex}} = 1 - \frac{T_a S_{\text{gen}}}{[1 - (T_a/T_s)]Q_s} \quad (6)$$

Here, the T_s is the sun temperature and is assumed to be 5900 K.

5. Results and Discussion

5.1. Taguchi OA Analysis of Controllable Factors on Thermal Efficiency and Temperature Difference of SAHs

The L_8 orthogonal design described by the Taguchi method was used for the optimization of the configuration of the SAH packed with iron wools (DPGSAHI) and mesh layers (DPGSAHM). The selected response of the parameters and the S/N ratios are shown in Table 3. As shown in Table 3, duplicates of eight runs were conducted, and relatively high S/N ratios were observed. A higher S/N ratio generally indicates a better specification, suggesting that more useful information (signal) than unwanted constraints (noise) occurred during the optimization process [19,28].

Table 3. L8 (7 two-level factors) orthogonal array for selected parameters and thermal efficiency.

Run	A	B	C	D	E	F	Thermal Efficiency (%)		Mean (%)	S/N Ratio
							Trial 1	Trial 2		
1	1	7	0.07	1	0.1	2	91.5	93.4	92.5	20.73
2	1	7	0.07	3	0.5	4	67.9	70.6	69.3	21.42
3	1	10	0.1	1	0.1	4	75.3	78.9	77.1	22.47
4	1	10	0.1	3	0.5	2	63.9	68.8	66.4	18.81
5	2	7	0.1	1	0.5	2	88.5	89.7	89.1	29.45
6	2	7	0.1	3	0.1	4	56.9	64.6	60.8	20.56
7	2	10	0.07	1	0.5	4	85.7	83.2	84.5	23.37
8	2	10	0.07	3	0.1	2	80.3	83.5	81.9	23.46

Notably, the lowest S/N ratio (18.81 dB) was observed in run four and in relatively low thermal efficiency (60.8%), indicating that the combination of the parameters in run four is hindered, hence not obviously maximizing the thermal efficiency of the DPGSAHI. A low standard deviation of ~ 2.8 and a very high CI of 96.5% were obtained, suggesting that each trial of thermal efficiency tend to be close to the mean value at a significance level of 0.035. Based on the ranking of the S/N ratio, the diameter of holes of plexiglass (D) has the largest effect on the SAH thermal efficiency, and the thickness of packing material (C) has the smallest effect on the overall thermal efficiency of the as-fabricated SAHs.

The graphical representation of the interaction effects of the parameters (Table 1) for the thermal efficiency and temperature difference at a constant mass flow rate of 0.024 kg/s and average solar intensity of 810.2 W/m² is shown in Figure 4. As noted in Figure 4a, parameter F significantly affects the thermal efficiencies of the as-fabricated SAHs. In all cases, the DPGSAHI exhibited a higher thermal efficiency as compared with the DPGSAHM. Notably, increasing the thickness of the packing material and the gap between the internal and plexi glasses does not affect the thermal efficiency of the SAHs. On the other hand, the DPGSAHI and DPGSAHM thermal efficiency decreased from 91.5% and 83.2% to 72% and 62%, respectively, when the thickness of the insulation material increased from 2 cm to 4 cm.

At a mean value of wind speed of 4.57 m/s, the temperature difference of the SAHs was obviously influenced by variation in the value of the parameters (Figure 4b). Increasing the values of parameters B, C and F significantly decreased the outlet temperature. As the thickness of the packing material and the gap between the internal and plexi glasses increased, the temperature difference decreased accordingly. The reason for this can be described as follows; as the thickness of the packing material increases, the rate of heat transfer to the flowing air decreases resulting in a decrease in convective heat transfer coefficient between the bed and the glasses and higher thermal losses [31].

Variation due to each parameter influences the thermal efficiency and temperature difference. Hence, analysis of variance (ANOVA) was applied to analyze the results of the orthogonal array experiment and determine the variations due to each parameter (Table 4).

In Table 5, the *p* and *F* values are important indicators in identifying the effect of each investigated parameter. Here, one numerator degree of freedom was observed for each parameter, and seven denominator degrees of freedom were observed for the total parameter. By looking at the *F*-distribution table with $\alpha = 5\%$, the SAH input parameter was considered to influence the response (thermal efficiency and temperature difference) if its *F*-value was higher than $F_{0.05}(1,7) = 5.59$. Moreover, if the *p*-value is less than $\alpha = 0.05$, the influence of that parameter on the response is significant [33].

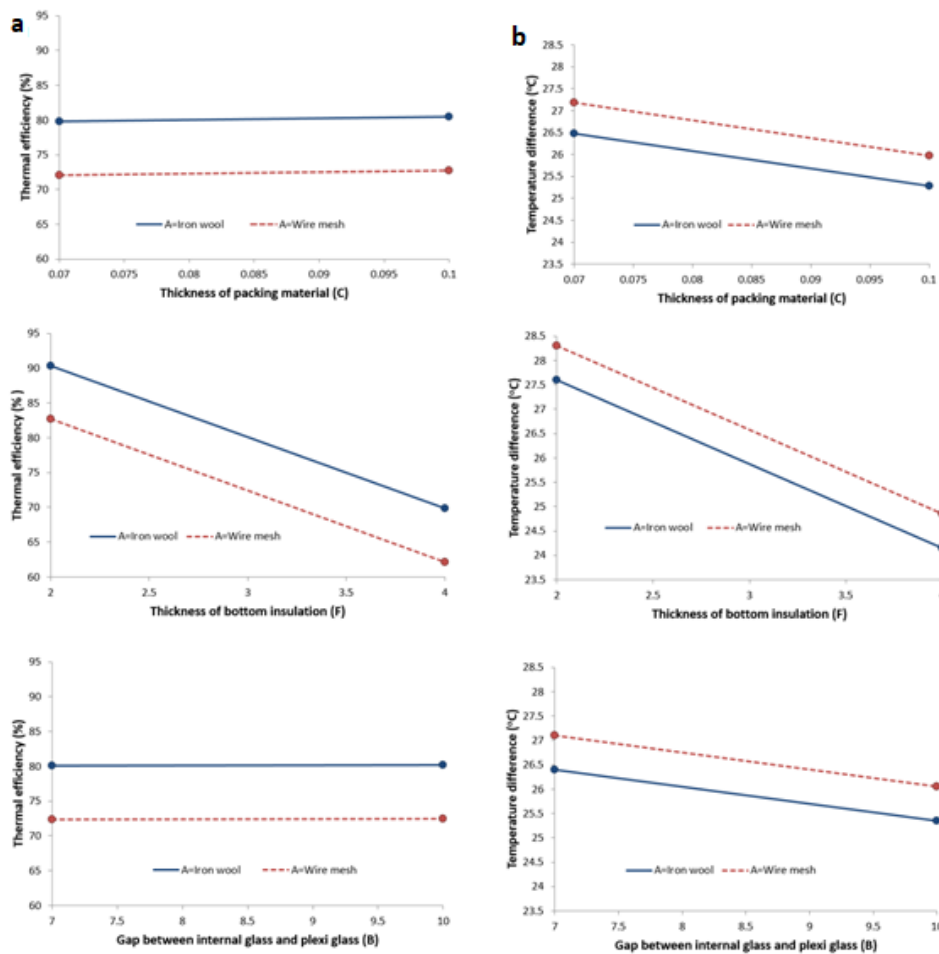


Figure 4. Interaction plots for the (a) thermal efficiency and (b) temperature difference based on Taguchi methods.

Table 4. Contribution of each parameter and ranking via the S/N ratio.

Level	A	B	C	D	F	Std. Dev	CI
1	20.86	23.04	22.25	24.01	23.11		
2	24.21	22.03	22.82	20.34	21.96		
Δ	3.35	1.01	0.57	3.67	1.15		
Rank	2	4	5	1	3	2.789	0.965

Note: $\Delta = \max - \min$, Std.Dev: Standard deviation, CI: Confidence interval.

It is evident that parameters A, D, E and F have F -values higher than 5.59 and p -values < 0.05 , confirming that these parameters have a significant statistical influence on the thermal efficiency and temperature difference of the DPGSAHI and DPGSAHM, at a 95% confidence level [34]. On the other hand, parameters B and C both have p -values ≥ 0.05 and F -values less than 5.59. This indicates that these parameters do not significantly influence the thermal efficiency and temperature difference of the as-fabricated SAHs. According to the ANOVA results and S/N ratio rank, the most significant parameter was found to be the diameter of holes of plexiglass (D) since a higher F -value signifies a more significant effect on the response [22]. The confirmation analysis indicated that the model has a larger Pred R^2 (97.6%) compared with the R^2 (95.6%). Hence the applied model is sufficiently suitable, and thus, the level of selected parameters can produce the best results with good predictability.

Table 5. ANOVA for the design of double-pass perforated glazed solar air heaters via Taguchi method.

Source	Seq SS	Adj SS	DF	Adj MS	F	p
Main	117.195		6			
Type of absorber material (A)	21.98	21.98	1	21.98	6.5029	0.038
Gap between internal glass and plexi glass (B)	2.205	2.205	1	2.205	0.6524	0.445
Thickness of packing material (C)	18.88	18.88	1	18.88	5.59	0.050
Diameter of holes of plexi glass (D)	27.905	27.905	1	27.905	8.2559	0.024
Distance between absorber material (E)	22.42	22.42	1	22.42	6.633	0.037
Thickness of bottom insulation (F)	23.805	23.805	1	23.805	7.0429	0.033
Regression	117.195	117.195	6	19.533		
Error	3.38	3.38	1	3.38		
Total	120.575		7			
R ²	0.9559					
Adj R ²	0.3412					
Pred R ²	0.9769					
Std Error	1.8385					
F	1.6043					
Sig F	0.5401					

DF: Degrees of Freedom; Seq SS: Sequential Sum of Squares; Adj SS: Adjusted Sum of Squares; Adj MS: Adjusted mean square.

5.2. Effect of Uncontrollable Factors on the Performance of the As-Fabricated DPGSAHI and DPGSAHM

Here, the effect of uncontrollable factors (solar intensity, inlet and ambient temperatures) was examined on the conventional and Taguchi optimized DPGSAHI and DPGSAHM. First, the wire mesh and iron wool were located in layers with the distance between them to decrease the pressure drop inside the SAHs. The official resources stated that the average hourly wind speed of Famagusta city was 4.57 m/s. The tests and readings started at 9:00 and continued until 16:00 on each day of the experiment. Figure 5 shows the change of solar flux intensity hour by hour against the local time per day in the current investigation. For reproducibility, duplicate studies were conducted, average results reported, and standard errors (less than 2%) were shown as error bars in the figures.

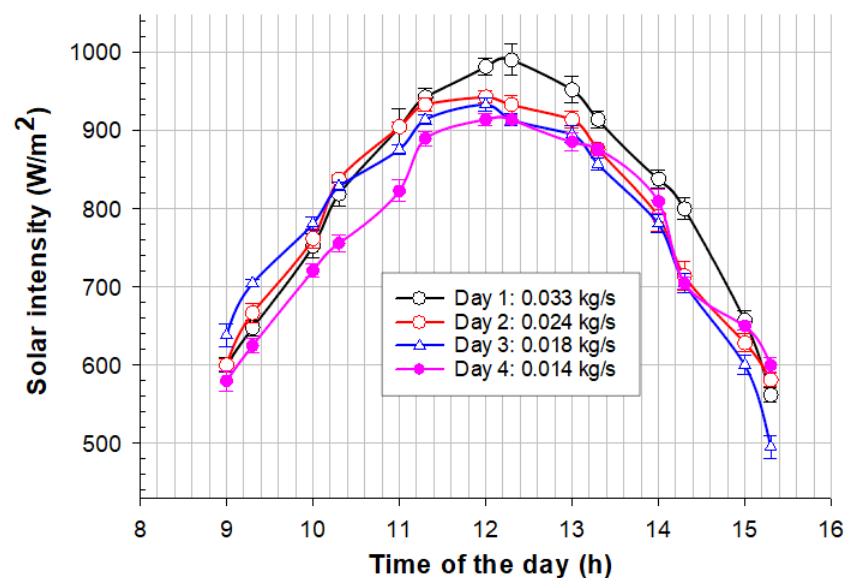


Figure 5. Change of solar intensity hour by hour versus various standard local time of four different days.

As expected, the solar radiation enhanced steadily from morning to a maximum value at noon and reduced afterwards until sunset. The measured solar intensities were relatively

stable throughout the studies, and for all days of the experiments, the average value of solar intensity is 792.5 W/m^2 while the maximum value is 990.5 W/m^2 . The variation of both inlet (ambient) and outlet temperature during the days of the experiments were examined at different mass flow rates. The ambient temperature was increasing slightly from morning until evening, and the mean value at a mass flow rate of 0.033 kg/s was $26.8 \text{ }^\circ\text{C}$, while the maximum value was $28.2 \text{ }^\circ\text{C}$.

The influence of mass flow rate on the DPGSAHI and DPGSAHM enhancement is demonstrated by the diurnal temperature difference ($\Delta T = T_{\text{out}} - T_{\text{in}}$) shown in Figure 6. As expected, ΔT increased with decreasing rate of air mass flow. The maximum amount of ΔT was observed between 10:30 h and 13:00 h of the apparent time, depending on the outdoor ambient conditions. It was also found that the DPGSAHI exhibited a higher magnitude of the ΔT in all mass flow rates investigated. This could be as a result of increased heat transfer area and higher porosity (98.3%) of the 48 iron pieces of wool in the DPGSAHI. The highest instantaneous and average peak values of ΔT obtained for the DPGSAHI were $21.2 \text{ }^\circ\text{C}$ and $16.4 \text{ }^\circ\text{C}$, respectively, at a mass flow rate of 0.033 kg/s . For the least flow rate of $\dot{m} = 0.014 \text{ kg/s}$, the maximum value of ΔT was $29.1 \text{ }^\circ\text{C}$ and the average value of ΔT was $24.3 \text{ }^\circ\text{C}$ (Figure 6a).

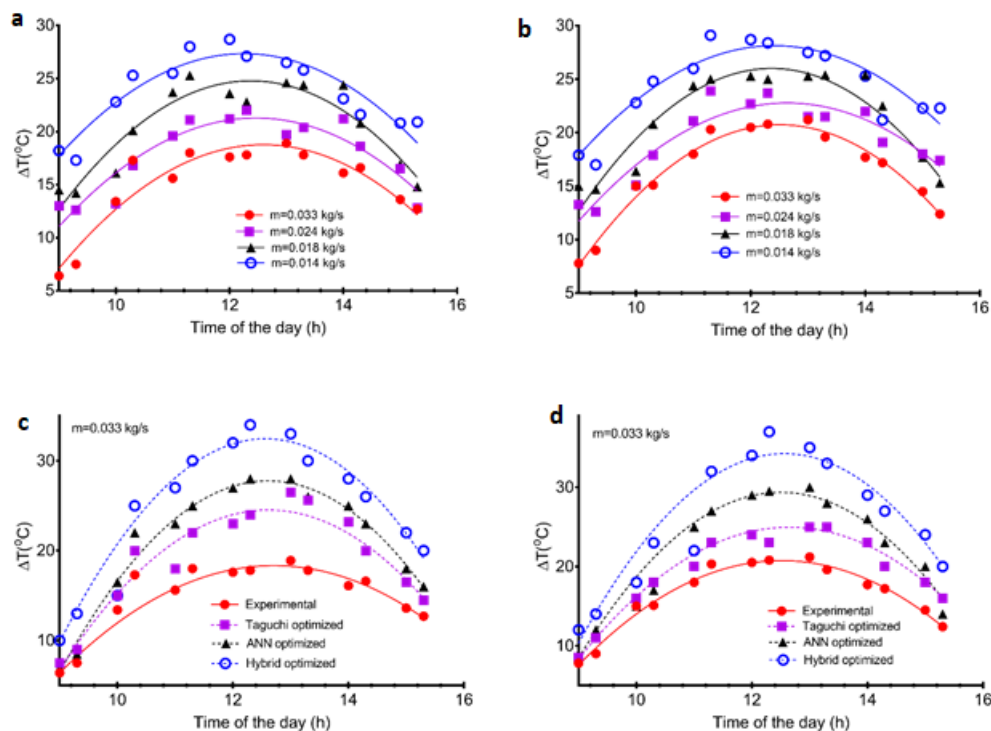


Figure 6. Temperature difference versus standard local time of the day at various mass flow rates for (a) DPGSAHM (b) DPGSAHI and temperature difference at optimized conditions for a mass flow rate of 0.033 kg/s for (c) DPGSAHM and (d) DPGSAHI.

In addition, the highest instantaneous peak and average ΔT achieved from the DPGSAHM were $18.9 \text{ }^\circ\text{C}$ and $14.9 \text{ }^\circ\text{C}$, correspondingly by a rate of mass flow of 0.033 kg/s . Whilst the peak and average value of ΔT at the rate of mass flow of 0.014 kg/s were $28.7 \text{ }^\circ\text{C}$ and $23.7 \text{ }^\circ\text{C}$, correspondingly (Figure 6b). As mentioned earlier, the configuration of the as-fabricated SAHs was optimized via Taguchi orthogonal arrays to obtain enhanced outlet air temperature and data obtained were fed into ANN architecture. It is interesting to note that the optimized parameters via Taguchi and ANN drastically enhanced the ΔT values of the DPGSAHI and DPGSAHM. The optimal conditions (Taguchi = B: 7cm, C: 0.07 cm, D: 1mm, E: 0.5 cm and F: 2cm) enhanced the ΔT of DPGSAHM by 40% from $18.9 \text{ }^\circ\text{C}$ to $26.5 \text{ }^\circ\text{C}$ at a mass flow rate 0.033 kg/s (Figure 6c). Moreover, combining the optimized ANN conditions (I: 880 W/m^2 , T_{air} : $26.5 \text{ }^\circ\text{C}$ and $\dot{m} = 0.0033 \text{ kg/s}$) with the Taguchi optimal

values generated a hybrid optimization (ANN-Taguchi), which significantly enhanced the ΔT by 75% (from 18.9 to 33 °C).

The enhancement acquired in ΔT is due to the increase in the area of heat transfer and reduction of heat loss. Reducing the thickness of the absorber material and distance between plexiglass and internal glass increased the air flow passages and reduced heat loss by convection, respectively. Specifically, as the air enters through the upper holes of the perforated plexiglass, it absorbs heat from the mesh layers as it propagates inside the collector, and due to the short distance between the plexiglass and the internal glass cover, the preheated air rapidly cools the internal cover, as a result, reduces the heat loss through the cover leading to increased ΔT [35]. A similar trend was observed for DPGSAHI where the hybrid optimization increased the ΔT of DPGSAHI by 27% from 28.9 to 37 °C (Figure 6d).

Comparatively, the maximum temperature difference ΔT recorded by the optimized DPGSAHI is relatively higher than those reported in the literature, considering the mass flow rates and solar intensity radiation. At the same solar radiation (880 W/m²) and lower mass flow rate (0.02 kg/s), Esen [36] recorded a maximum temperature of 23 °C from a double-flow flat plate SAH with obstacles. Ramadan et al. [10] reported that the maximum ΔT of double-pass SAH at the solar intensity of 850 W/m² was 35 °C by the $\dot{m} = 0.0105$ kg/s. Furthermore, El-khawajah et al. [11] obtained 25.5 °C as the peak value of ΔT of two-fins SAH containing wire mesh as an absorber plate with a mass flow rate of $\dot{m} = 0.042$ kg/s.

The thermal efficiencies against hours of the day at various mass flow rates are illustrated in Figure 7. The thermal efficiencies enhance with an increment in the mass flow rate depending on the ambient conditions of the day. These observations are similar to our previous report [4] and those of Mahmood et al. [7] and Kabeel et al. [37]. The maximum efficiency obtained from the DPGSAHM and DPGSAHI were 81.4%, and 91.3% at 13:00, respectively, with an air mass flow rate of 0.033 kg/s. Depending on the inlet air temperatures and solar intensity, the thermal efficiency enhanced from morning to evening continuously. As the behaviour of input air temperature, in most cases, the thermal efficiency was observed to be enhanced by the standard local time of the day from daybreak to sunset, this attributed to the heat accumulated inside the porous media (wire mesh and iron wool) energy in the matrix bed. However, an inconsiderable reduction in the thermal efficiency was observed in the afternoon for high mass flow rates. Particularly, the DPGSAHI at a mass flow rate of 0.033 kg/s decreased from 91.3% to ~90% at 15:00. After 12:00, the solar intensity tends to diminish; meanwhile, the air mass flow rate carries the same amount of energy continuously, which is the energy absorbed from the porous media and the energy received from the sun [7]. In all cases investigated in the current study (Figure 7a,b), the thermal efficiency in the iron wool-based double-pass SAH (DPGSAHI) was higher than that of a wire mesh layer-based double-pass SAH (DPGSAHM).

The comparison of the average efficiencies of obtained data for double-pass SAHs with the present research indicates there is an enhancement in the proposed SAHs (Figure 8). Notably, the average thermal efficiencies of DPGSAHI, DPGSAHM and hybrid optimized DPGSAHI (~82–97%) at relatively lower mass flow rates (0.014–0.033 kg/s) were found to be comparatively higher than the double-pass with porous media (steel wool) reported by Sopian et al. [3] and steel wire mesh based double-pass SAH reported by Omojaro and Aldabbagh [5]. Generally, under optimized conditions, increasing the number of iron wool (from 32 to 48) and wire mesh layers (10 to 15) increases the contact surface area in the SAH and significantly enhances the efficiency of the as-fabricated SAHs. Moreover, the low spacing between the plexiglass and the internal glass cover increases the average air flow velocity and subsequently increases the heat transfer coefficient.

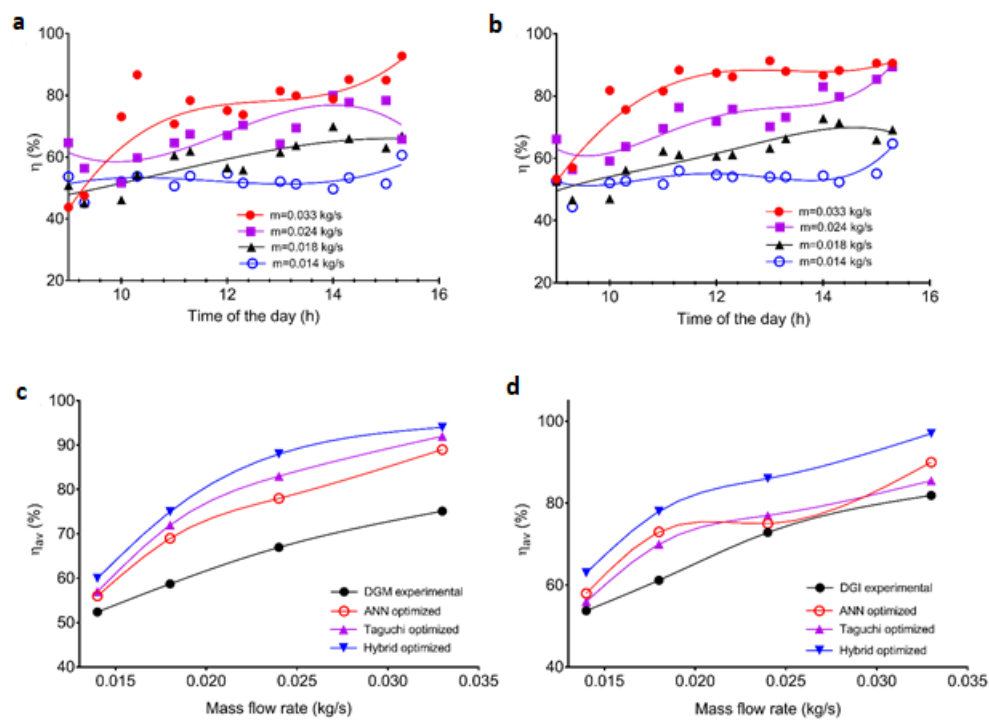


Figure 7. Change of collector thermal efficiency at various mass flow rates (a) DPGSAHM (b) DPGSAHI at 990 W/m^2 and 14.2 m/s and optimized results compared with (c) average DPGSAHM and (d) average DPGSAHI experimental efficiencies.

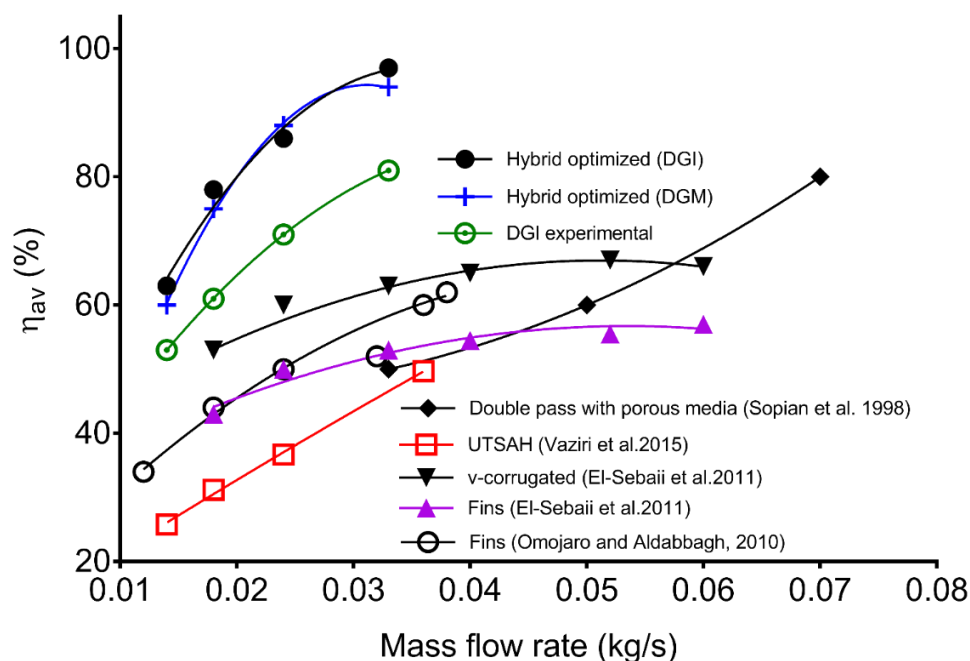


Figure 8. Average thermal efficiency comparison between the hybrid optimized DPGSAHI and DPGSAHM with reported SAHs in the literature.

The irreversibility and exergy efficiency versus mass flow rate for DPGSAHI, DPGSAHM and hybrid optimized SAHs are shown in Figure 9. Obviously, the exergy efficiencies show a minimum in non-optimized DPGSAHI and DPGSAHM (Figure 9a,b), 1.21% for DPGSAHI experimental and 1.45% for DPGSAHM at 0.033 kg/s whereas, $\sim 3\%$ and 2.4% exergy efficiencies were obtained for the hybrid optimized DPGSAHM and DPGSAHI, respectively. Notably, the exergy efficiency became greater at a \dot{m} (7.1% for DPGSAHI at

0.014 kg/s) and mitigated with increments in rate mass flow, compatible by the study of Velmurugan and Kalaivanan [32] and Chouksey and Sharma [31].

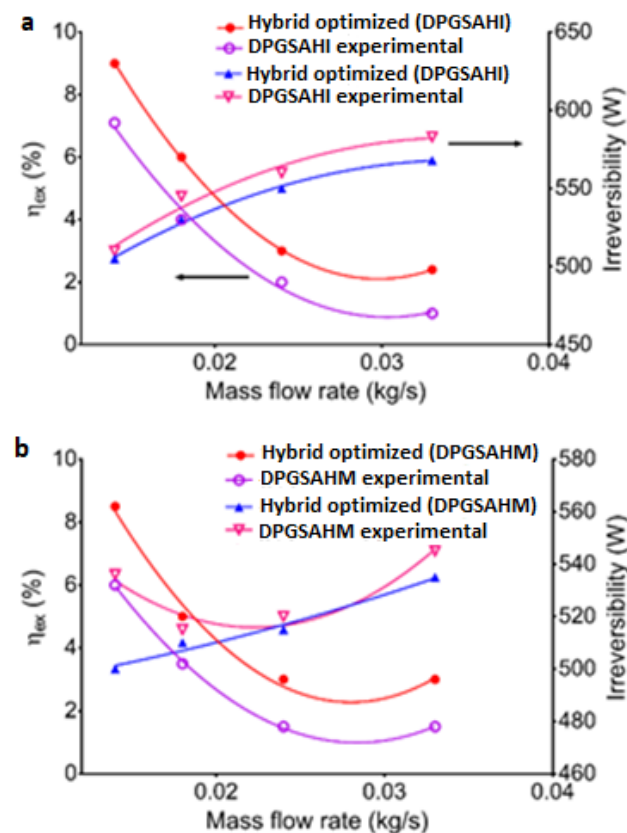


Figure 9. Change of exergy efficiency and irreversibility with various mass flow rates.

As indicated in Figure 6, the ΔT between the absorber plates and the current of air was greater at a lower mass flow rate of 0.014 kg/s. Therefore, the heat transfer to the flowing air was at the highest value, subsequently resulting in maximum exergy conversion and exergy efficiency (9–8.5% for hybrid optimized at 0.014 kg/s). At $\dot{m} = 0.014$ kg/s, the irreversibility was 510 W for DPGSAHI and 535 W for DPGSAHM demonstrating a greater loss in the DPGSAHM system. In both cases, the entropy generation rate was observed to increase exponentially with an increase in mass flow rate. Hence the irreversibility was less at a lower level of mass flow rate, possibly due to the highest value of existing energy transfer [38].

5.3. Cost Analysis for the Heat Gained

Here, the total cost of the hybrid optimized DPGSAHI and DPGSAHM at a fixed mass flow rate and the quantity of useful heat gained was estimated. The fixed cost (F_c), variable cost (V_c) and straight-line depreciation (SL) were considered. $\dot{m} = 0.033$ kg/s. Table 6 shows the fixed cost and the following points were considered during the cost–benefit analysis:

- One year of operation was assumed to equal 350 days.
- Ten years' straight-line depreciation method was considered at 2%.
- Miscellaneous charges, including labour and maintenance costs were excluded.
- The number of working hours is 8 h/day.
- The expected life time (n_y) is assumed 15 years.

Table 6. Components and cost of the hybrid optimized DPGSAHI and DPGSAHM systems.

Component	Cost (\$) ^a		Q _{av} (kW/Year) ^b	
	DPGSAHI	DPGSAHM	DPGSAHI	DPGSAHM
Wooden box	5	5	1743.5	1472.9
Dimer	13.3	13.3		
PV-system	280	280		
Thermal insulation polystyrene	2	2		
Fan blower	66.7	66.7		
Plexi glass	15.5	15.5		
Pipe	4.4	4.4		
Internal glass cover	11.1	11.1		
Iron wool	25			
Steel wire mesh layer		5		
Total fixed cost	423	403		

^a: Unit prices for the Turkish Republic of Northern Cyprus market in May 2018 at 1\$ = 4.4TL. ^b: Calculated from Equation (6), using η_{avd} of 82 and 97% for hybrid optimized DPGSAHM and DPGSAHI, respectively.

The average heat produced per year (Q_{av}) was calculated as follows:

$$Q_{av} = I_{av} \times A_{ac} \times \eta_{avd} \times \text{no. of days per year} \times \text{no. of hours per day} \quad (7)$$

The variable cost was $V_c = 0.13 \times (F_c - \text{PV system cost})$, the total cost $T_C = F_c + V_c + \text{SL}$ and the total cost per year was calculated using $C_y = T_C/n_y$.

5.3.1. For Hybrid Optimized DPGSAHI

Considering mass flow rate of 0.033 kg/s, the cost of useful kW was computed as follows, $F_c = 423$ \$, then $T_C = 423 + (0.13 \times 143 \times 15) + 8.46 = 710.31$ \$. Then, C_y is 47.35 \$/year. As presented in Table 6, the Q_{av} of DPGSAHI was calculated as 1743.5 kW/year, then the cost per one kW is 0.027 \$.

5.3.2. For Hybrid Optimized DPGSAHM

Similarly, considering $\dot{m} = 0.033$ kg/s, the $F_c = 403$ \$ was obtained, then $T_C = 403 + (0.13 \times 123 \times 15) + 8.06 = 650.91$ \$. Then, C_y is 43.39 \$/year. The Q_{av} of DPGSAHM was calculated as 1472.9 kW/year, then the cost per one kW is 0.029 \$. It is worth mentioning that the maximum daily energy efficiency (82–97%) delivered by the hybrid optimized DPGSAHI and DPGSAHM at mass flow rate of 0.033 kg/s and the average cost per kW (0.028 \$) of useful heat gained was comparatively higher than the baffled glazed-bladed entrance air heater ($\eta_{avd} = 83.8\%$ and 0.00733 \$ at mass flow rate of 0.04 kg/s) reported by Kabeel et al. [37].

6. Conclusions

Double-pass perforated glazed solar air heaters (SAHs) packed with wire mesh layers (DPGSAHM), and iron wools (DPGSAHI) were experimentally investigated. The effects of air mass flow rate on the thermal efficiency, exergy efficiency and outlet temperature were surveyed. The as-fabricated SAHs exhibited a decrease in the thermal efficiency as the mass flow rate was decreased from 0.033 kg/s to 0.014 kg/s. It was found that for the same mass flow rate (0.024 kg/s), the DPGSAHI has higher efficiency (89.3%) compared to the DPGSAHM (~80%). Furthermore, the maximum temperature difference (ΔT) for the DPGSAHI (29.1 °C) slightly exceeded the DPGSAHM (28.7 °C) for the identical mass flow rate (0.014 kg/s). As expected, the highest value of exergy efficiency (η_{ex}) for various types of solar air heater was gained at the minimum rate of air mass flow. A substantial enhancement in the temperature difference (75%), thermal efficiency (1.25%) and exergy efficiency (2.4%) was achieved when the DPGSAHM and DPGSAHI were optimized by the hybrid procedure (Taguchi-artificial neural network). Notably, the average

thermal efficiencies and the average cost per kW gained (0.028 \$) herein are found to be comparatively higher than the double-pass SAHs with porous media (steel wool and wire mesh layers) reported in the literature.

Results herein indicate that the variation in efficiency of the ANN and Taguchi method was 1.95% and 2.14%, respectively. Importantly, under optimal conditions, the ANN and Taguchi method have an increment of 7.98–6.45% and 6.89–5.35% in thermal efficiency of DPGSAHI and DPGSAHM, respectively, when compared with physical experimental results.

Author Contributions: Conceptualization, R.V.; methodology, R.V. and A.A.O.; software, A.A.O.; validation, R.V.; formal analysis, R.V. and A.A.O.; data curation, R.V.; writing—original draft preparation, R.V. and A.A.O.; writing—review and editing, M.S., R.T., M.H.A. and A.I.; supervision, M.S. and M.H.A. All authors have read and agreed to the published version of the manuscript.

Funding: This research received no external funding.

Institutional Review Board Statement: Not applicable.

Informed Consent Statement: Not applicable.

Data Availability Statement: The data presented in this study are available with the permission of authors.

Conflicts of Interest: The authors declare no conflict of interest.

Nomenclature

C_p	specific heat of the air (kJ/kg.K)
C_y	total cost per year
F_c	fixed cost
I	solar intensity (W/m ²)
\dot{m}	air flow rate (kg/s)
n	the number of tests
n_y	expected life time
Q_{av}	average heat produced per year
Q_s	Incident energy in the collector area (kW)
r	radius (m)
R^2	coefficient of determinations
SL	straight-line depreciation
S/N	signals to noise
S_{gen}	entropy, kJ.kg ⁻¹ K ⁻¹
T_a	ambient temperature (°C)
T_{air}	temperature of air (°C)
T_{in}	inlet temperature (°C)
T_{out}	outlet temperature (°C)
T_s	the temperature of sun (°C)
T_C	total cost
V	velocity (m/s)
V_c	variable cost
x_n	input variable
X_0	actual value of input variables
X_{max}	maximum values of input variables
X_{min}	minimum values of input variables
X_n	normalized value
y	response
Greek Symbols	
ΔT	temperature difference ($T_{out} - T_{in}$)(°C)
\emptyset	porosity
ω_r	uncertainty
η	efficiency of the solar collector

η_{ex}	exergetic efficiency
Abbreviation	
ABC	artificial bee colony
ANN	artificial neural network
ANOVA	analysis of variance
CI	Confidence interval
DPGSAH	double-pass perforated glazed solar air heater
DPGSAHM	double-pass perforated glazed solar air heaters packed with wire mesh layers
DPGSAHI	double-pass perforated glazed solar air heaters packed with iron wools
DPSAH	double-pass solar air heater
FDM	finite difference method
GA	genetic algorithm
LM	Levenberg–Marquardt
OA	orthogonal arrays
PG	perforated plexiglass
QNM	Quasi–Newton method
RMSE	root means square error
SAH	solar air heater
SNR	signal-to-noise ratio
Std.Dev	Standard deviation

References

- Varun; Saini, R.P.; Singal, S.K. A review on roughness geometry used in solar air heaters. *Sol. Energy* **2007**, *81*, 1340–1350. [[CrossRef](#)]
- Alta, D.; Bilgili, E.; Ertekin, C.; Yaldiz, O. Experimental investigation of three different solar air heaters: Energy and exergy analyses. *Appl. Energy* **2010**, *87*, 2953–2973. [[CrossRef](#)]
- Sopian, K.; Alghoul, M.A.; Alfegi, E.M.; Sulaiman, M.Y.; Musa, E.A. Evaluation of thermal efficiency of double-pass solar collector with porous–nonporous media. *Renew. Energy* **2009**, *34*, 640–645. [[CrossRef](#)]
- Vaziri, R.; Ilkan, M.; Egelioglu, F. Experimental performance of perforated glazed solar air heaters and unglazed transpired solar air heater. *Sol. Energy* **2015**, *119*, 251–260. [[CrossRef](#)]
- Omojaro, A.P.; Aldabbagh, L.B.Y. Experimental performance of single and double pass solar air heater with fins and steel wire mesh as absorber. *Appl. Energy* **2010**, *87*, 3759–3765. [[CrossRef](#)]
- Aldabbagh, L.B.Y.; Egelioglu, F.; Ilkan, M. Single and double pass solar air heaters with wire mesh as packing bed. *Energy* **2010**, *35*, 3783–3787. [[CrossRef](#)]
- Mahmood, A.J.; Aldabbagh, L.B.Y.; Egelioglu, F. Investigation of single and double pass solar air heater with transverse fins and a package wire mesh layer. *Energy Convers. Manag.* **2015**, *89*, 599–607. [[CrossRef](#)]
- Karmare, S.V.; Tikekar, A.N. Experimental investigation of optimum thermohydraulic performance of solar air heaters with metal rib grits roughness. *Sol. Energy* **2009**, *83*, 6–13. [[CrossRef](#)]
- Kumar, R.A.; Babu, G.B.; Mohanraj, M. Experimental investigations on a forced convection solar air heater using packed bed absorber plates with phase change materials. *Int. J. Green Energy* **2017**, *14*, 1238–1255. [[CrossRef](#)]
- Ramadan, M.R.I.; El-Sebaei, A.A.; Aboul-Enein, S.; El-Bialy, E. Thermal performance of a packed bed double-pass solar air heater. *Energy* **2007**, *32*, 1524–1535. [[CrossRef](#)]
- El-Khawajah, M.F.; Egelioglu, F.; Ghazal, M. Finned single-pass solar air heaters with wire mesh as an absorber plate. *Int. J. Green Energy* **2015**, *12*, 108–116. [[CrossRef](#)]
- Paisarn, N. On the performance and entropy generation of the double-pass solar air heater with longitudinal fins. *Renew. Energy* **2005**, *30*, 1345–1357.
- Tchinda, R. A review of the mathematical models for predicting solar air heaters system. *Renew. Sustain. Energy Rev.* **2009**, *13*, 1734–1759. [[CrossRef](#)]
- Saxena, A.; Varun; El-Sebaei, A.A. A thermodynamic review of solar air heaters. *Renew. Sustain. Energy Rev.* **2015**, *43*, 863–890. [[CrossRef](#)]
- Bhattacharyya, S.; Sarkar, D.; Roy, R.; Chakraborty, S.; Goel, V.; Almatrafi, E. Application of new artificial neural network to predict heat transfer and thermal performance of a solar air-heater tube. *Sustainability* **2021**, *13*, 7477. [[CrossRef](#)]
- Alam, W.M.; Souayeh, B. Parametric CFD Thermal performance analysis of full, medium, half and short length dimple solar air tube. *Sustainability* **2021**, *13*, 6462. [[CrossRef](#)]
- Panda, S.; Singla, R.K.; Das, R.; Martha, S.C. Identification of design parameters in a solar collector using inverse heat transfer analysis. *Energy Convers. Manag.* **2014**, *88*, 27–39. [[CrossRef](#)]
- Das, R.; Singh, K.; Akay, B.; Gogoi, T.K. Application of artificial bee colony algorithm for maximizing heat transfer in a perforated fin. *J. Proc. Mech. Eng.* **2016**, *232*, 38–48. [[CrossRef](#)]

19. Oladipo, A.A.; Gazi, M. Two-stage batch sorber design and optimization of biosorption conditions by Taguchi methodology for the removal of acid red 25 onto magnetic biomass. *Korean J. Chem. Eng.* **2015**, *32*, 1864–1878. [[CrossRef](#)]
20. Chamoli, S.; Chauhan, R.; Thakur, N.S.; Saini, J.S. A review of the performance of double pass solar air heater. *Renew. Sustain. Energy Rev.* **2012**, *16*, 481–492. [[CrossRef](#)]
21. Kuo, C.F.J.; Su, T.L.; Jhang, P.R.; Huang, C.Y.; Chiu, C.H. Using the Taguchi method and grey relational analysis to optimize the flat-plate collector process with multiple quality characteristics in solar energy collector manufacturing. *Energy* **2011**, *36*, 3554–3562.
22. Gazi, M.; Oladipo, A.A.; Ojoro, Z.E.; Gulcan, H.O. High-performance nanocatalyst for adsorptive and photo-assisted Fenton-like degradation of phenol: Modeling using artificial neural networks. *Chem. Eng. Commun.* **2017**, *204*, 729–738. [[CrossRef](#)]
23. Omojaro, P.; Nwulu, N.I.; Ilkan, M. Deploying an Artificial Neural Network Model for Solar Air Heating Modelling. *Int. J. Inf.* **2013**, *16*, 3249–3257.
24. Ghritlahre, H.K.; Prasad, R.K. Investigation of thermal performance of unidirectional flow porous bed solar air heater using MLP, GRNN, and RBF models of ANN technique. *Therm. Sci. Eng. Prog.* **2018**, *6*, 226–235. [[CrossRef](#)]
25. Ghritlahre, H.K.; Chandrakar, P.; Ahmad, A. Application of ANN model to predict the performance of solar air heater using relevant input parameters. *Sustain. Energy Technol. Assess.* **2020**, *40*, 100764. [[CrossRef](#)]
26. Shetty, S.P.; Nayak, S.; Kumar, S.; Karanth, K.V. Thermo-hydraulic performance prediction of a solar air heater with circular perforated absorber plate using Artificial Neural Network. *Therm. Sci. Eng. Prog.* **2021**, *23*, 100886. [[CrossRef](#)]
27. Lin, H.C.; Su, C.T.; Wang, C.C.; Chang, B.H.; Juang, R.C. Parameter optimization of continuous sputtering process based on Taguchi methods, neural networks, desirability function, and genetic algorithms. *Expert Syst. Appl.* **2012**, *39*, 12918–12925. [[CrossRef](#)]
28. Chamoli, S. A Taguchi approach for optimization of flow and geometrical parameters in a rectangular channel roughened with V down perforated baffles. *Case Stud. Therm. Eng.* **2015**, *5*, 59–69. [[CrossRef](#)]
29. Oladipo, A.A.; Vaziri, R.; Abureesh, M.A. Highly robust AgIO₃/MIL-53 (Fe) nanohybrid composites for degradation of organophosphorus pesticides in single and binary systems: Application of artificial neural networks modelling. *J. Taiwan Inst. Chem. Eng.* **2018**, *83*, 133–142. [[CrossRef](#)]
30. Holman, J. *Experimental Methods for Engineers*, 7th ed.; McGraw-Hill: New York, NY, USA, 1989.
31. Chouksey, V.K.; Sharma, S.P. Performance analysis of optically semi-transparent material packed-bed solar air heater. *Int. J. Thermodyn.* **2017**, *20*, 44–57. [[CrossRef](#)]
32. Velmurugan, P.; Kalaivanan, R. Energy and exergy analysis of multi-pass flat plate solar air heater-An analytical approach. *Int J. Green Energy* **2015**, *12*, 810–820. [[CrossRef](#)]
33. Sholahudin, S.; Han, H. Simplified dynamic neural network model to predict heating load of a building using Taguchi method. *Energy* **2016**, *115*, 1672–1678. [[CrossRef](#)]
34. Acir, A.; Canli, M.E.; Ata, I.; Cakiroglu, R. Parametric optimization of energy and exergy analyses of a novel solar air heater with grey relational analysis. *Appl. Therm. Eng.* **2017**, *122*, 330–338. [[CrossRef](#)]
35. Nowzari, R.; Aldabbagh, L.B.Y.; Egelioglu, F. Single and double pass solar air heaters with partially perforated cover and packed mesh. *Energy* **2014**, *73*, 694–702. [[CrossRef](#)]
36. Esen, H. Experimental energy and exergy analysis of a double-flow solar air heater having different obstacles on absorber plates. *Build. Environ.* **2008**, *43*, 1046–1058. [[CrossRef](#)]
37. Kabeel, A.E.; Hamed, M.H.; Omara, Z.M.; Kandel, A.W. On the performance of a baffled glazed-bladed entrance solar air heater. *Appl. Eng.* **2018**, *139*, 367–375. [[CrossRef](#)]
38. Farahat, S.; Sarhaddi, F.; Ajam, H. Exergetic optimization of flat plate solar collectors. *Renew. Energy* **2009**, *34*, 1169–1174. [[CrossRef](#)]